Ocean Engineering
December 2022, Volume 265 Pages 112582 (13p.)
https://doi.org/10.1016/j.oceaneng.2022.112582
https://archimer.ifremer.fr/doc/00795/90736/

Sea states influence on the behaviour of a bottom mounted full-scale twin vertical axis tidal turbine

Moreau Martin [1, 2], Germain Grégory [1, *], Maurice Guillaume [2], Richard Aloïs [2]

[1] Ifremer, Marine Hydrodynamic Laboratory, LHyMar, 150 Quai Gambetta, 62200 Boulogne-sur-Mer, France
[2] HydroQuest SAS, 16 Chemin de Malacher, 38240 Meylan, France

* Corresponding author : Grégory Germain, email address : gregory.germain@ifremer.fr

guillaume.maurice@hydroquest.net

Abstract :

As only a few tidal turbine developers have reached full-scale installation, the community lacks clear feedback on the validity of development tools to predict in-situ behaviour. From 2019 to 2021, HydroQuest tested its first 1 MW capacity bottom mounted twin vertical axis tidal turbine (VATT) OceanQuest at the Paimpol-Bréhat site, off the coast of Brittany, France. Thus, two years of operational data are available to analyse the behaviour of the full-scale VATT at sea. After describing the environmental conditions and the average performance of the machine, the wave effect on the turbine response is studied. The presence of strong waves multiplies almost by a factor 3 the fluctuation intensities of the torque, the rotational speed of the rotors and the turbine drag, without affecting significantly the mean quantities. The strong coherence between the loads and velocity spectra in the wave frequencies range indicates that the increase of fluctuation intensities is directly due to the periodic loads of surface waves.

Highlights

► In-situ measurements on a bottom mounted full-scale twin vertical axis tidal turbine. ► Sea states effect on turbine performance. ► Strong waves multiply the load fluctuation intensities by a factor 3. ► Strong coherence between loads and velocity spectra around the wave peak frequency.

Keywords : Tidal energy, Vertical axis turbine, Cross-flow, In-situ measurement, Waves effect

Nomenclature and abbreviations

ADCP	Acoustic Doppler Current Profiler
AFI	Rotation Against the Flow at the Inside, along the central fairing
Q	Torque
Hs	Significant wave height
FI	Fluctuation Intensity (standard deviation divided by mean of the quantity)
FT	Fourier Transform
Fx	Load in the turbine heading direction, in the main flow direction
Fy	Load in the direction transverse to the turbine heading
HATT	Horizontal Axis Tidal Turbine
IEC TS	International Electrotechnical Commission Technical Specification
MC	Measurement Campaign
k	Control law parameter
R	Rotor radius
TEC	Tidal Energy Converter
Tp	Waves peak period
U_{cap}	Velocity averaged (cubic power weighted) in time over 10 minutes and in space over the capture area
U_{HQ}	Velocity measured above the TEC by the ADCP-HQ (arithmetic average in space)
VATT	Vertical Axis Tidal Turbine
ω	Rotational speed
WFI	Rotation With the Flow at the Inside, along the central fairing

1. Introduction

In the past decade, a large amount of work has been performed on lab-scale tidal turbines, whether horizontal axis (HATT) [1, 2, 3] or vertical axis (VATT) [4, 5, 6]. In particular, [7] showed that the flow fluctuations induced either by the presence of turbulence or waves increases torque and loads fluctuations of the lab-scale HATT, without shifting significantly the mean values compared to laminar current alone. Draycott et al. [8] also demonstrated that loads and power fluctuations of a HATT strongly mimic both the temporal and spectral form of the generated focused wave condition at lab-scale and [9] gives a physical interpretation of the power-law scaling in the inertial range of the turbine power spectra.

However, there is a lack of feedback on the validity of lab-scale results extrapolation to full-scale [10] since few tidal turbine developers have achieved full-scale deployment [11, 12, 13] even if there are currently some plans to expand to commercially sized projects with farms of turbines [14, 15]. Coles et al. [16] report that 18 MW of tidal stream capacity has been installed in the UK since 2008. The majority of the systems have been monitored and controlled in order to evaluate their performances.

The incident velocity measurement is an important input in the performance characterisation of TECs. The International Electrotechnical Commission Technical Standards (IEC TS) requires only a single bottom mounted Acoustic Doppler Current Profiler (ADCP) to investigate the vertical distribution of the current velocities for resource and power performance assessment [17]. The mean incident velocity is then computed under the assumption of flow homogeneity on the TEC width. However, mean incident velocity assessment from single ADCP measurements is sensitive to many sources of uncertainties associated mainly with the beams spreading, their misalignment as well as the tilt of the device and the turbulence intensity [18]. Five beam ADCP, including a vertical one, can also be used to measure surface waves and turbulence of the flow [19]. Bouferrouk et al. [20] show that, except for peak period, spectral estimates of wave height, mean energy period and spectral bandwidth from an ADCP vertical beam agree well with estimates from co-located directional wave buoys. For turbulence kinetic energy measurement, methods for separation of wave and turbulence effects on the fluctuating part of the velocity needs to be used [21, 22]. In [23], large-eddy simulation of a high Reynolds number flow over a rough sea bed is performed and used to assess the accuracy of two coupled 4-beam ADCPs system forming an 8-beam arrangement. Results are globally satisfying and confirm the relevance and efficiency of the tested 8-beam configuration for the characterisation of turbulence. The quality of the results near the seabed is lower however, which questions the accuracy of ADCP measurements in the bottom of the water column, especially if only one 4-beam ADCP is used to characterise the incident flow.

Since 2008, EDF has developed a test site for Tidal Energy Converters (TEC) with on- and off-shore infrastructures off Bréhat island, near Paimpol, France [24, 25, 26]. The first program was conducted by OpenHydro who tested three generations of its TEC, which should have led to the grid-connection of two 1 MW turbines. This program ended in 2017 leaving EDF's infrastructures available. In the spring of 2019, HydroQuest installed its own 1 MW capacity TEC demonstrator, *OceanQuest*, at the test site.

For this company, the installation at sea comes after a decade of development of twin contra-rotative vertical axis current energy converters, inspired by Darrieus and Achard turbines [27]. Before 2019, numerical simulations [28, 29], tank tests and installations in rivers provided experience to the developer. The installation at sea of the turbine is an important step forward in the development of the technology. Following this installation, a dedicated flow measurement campaign enabled the certification of *OceanQuest*'s power curve by Bureau Veritas according to IEC TS 62600-200 [17]. After two years of successful tests at sea, the demonstrator was retrieved to be inspected and dismantled in October 2021 (Fig. 1).

In this paper, we describe the design of the ducted twin VATT and the environmental conditions present at Paimpol-Bréhat test site. Then, the performance and the behaviour of the demonstrator are analysed in the temporal and spectral domains with regard to the sea states.

(a) Gravity base at decommissioning

(b) Turbine at Cherbourg quayside for inspection

Figure 1: *OceanQuest* retrieval from Paimpol-Bréhat test site in October 2021.

2. Materials and methods

The first part of this section presents the main parameters of *OceanQuest* and its embedded instrumentation for performance and mechanical behaviour measurements. Then, we detail the method used to characterise the flow using Acoustic Current Doppler Profilers (ADCP). Finally, we introduce the process implemented in this study to select relevant data among the 21 months of operation to study the waves effects on the VATT behaviour.

2.1. Vertical axis tidal turbine demonstrator

OceanQuest is composed of two independent counter-rotative vertical axis rotor columns (Fig. 2 (a)). At flood tide, the rotors rotate Against the Flow at the Inside (AFI), along the central fairing, whereas they rotate With the Flow at the Inside (WFI) at ebb tide (Fig. 2 (b)). The columns are mounted in a $H = 9.8$ m high and $W = 24.7$ m wide mechanical structure made of fairings and plates. Each column is made of two levels of rotors fixed to the same shaft with a 60° phase difference between them, and each rotor is made of three 3.8 m high blades with a NACA 0018 profile projected on the swept cylinder. The rotors radius (R) is 4 m with blades chord (c) of 1.47 m which leads to a solidity (s, Eq. 1) of 1.1.

$$s = \frac{N.c}{R} \tag{1}$$

Permanent Magnet Generators (PMG) are placed at the top of each column shaft on the mechanical structure. The PMG pilot the rotors by an open loop torque control based on the rotational speed measurement following the control law defined in Eq. 2 with Q the torque, ω the rotational speed, k the control parameter and D_0 a constant that depends on the turbine's specifications. The output power is limited to its nominal value P_{max} by limiting the torque, and so increasing the rotational speed (Eq. 3).

$$Q = k.D_0.\omega^2 \tag{2}$$

$$Q = \frac{P_{max}}{\omega} \tag{3}$$

The turbine structure is fixed on the vertical mast of a tripod gravity base. The electric conversion elements are installed in a watertight chamber, located inside the upper central fairing. The turbine is

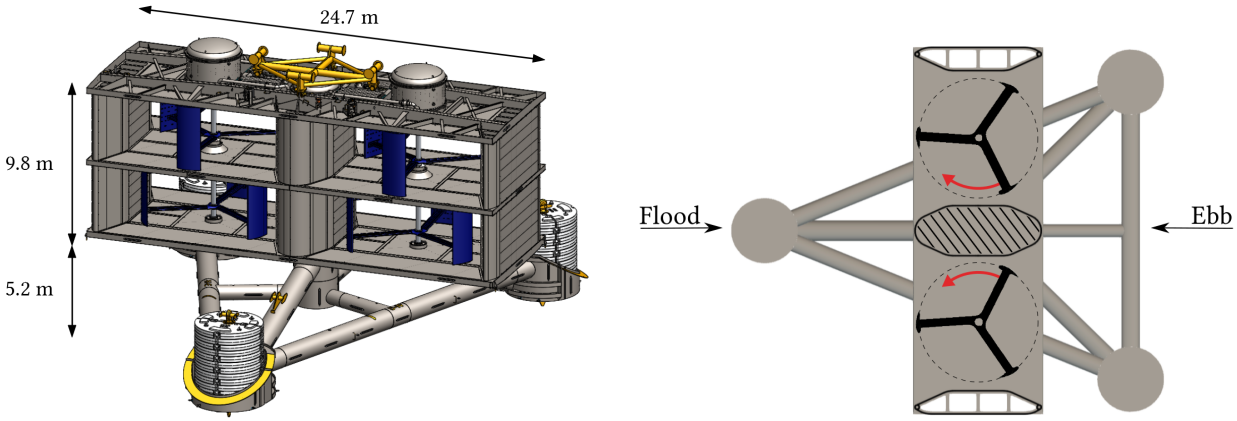

(a) Full CAD view of the demonstrator (b) Turbine's rotation direction on a sectional scheme

Figure 2: *OceanQuest* synthesis images.

connected to shore with a 16 km long optical fibre for generators control and measurement signals, and the electric power is dissipated in power banks.

The electrical current and voltage at the generators output are both measured at 1 Hz to calculate the active power converted by the turbine. Knowing the electrical and mechanical parameters of the machine, the current measurement is also used to model the mechanical torque on the rotor shafts. The rotational speed is measured on each shaft by position encoders at 1 Hz. Besides, strain gauges are placed on the vertical mast of the base to measure deformations in flexion and torsion. A calibration process was carried out on the dock before the immersion of the demonstrator to estimate the shear load at the top of the base's mast (where the turbine is fixed) from the measured strains. Due to the base asymmetry with regard to the transverse axis, the transformation matrix for axial loads (Fx, in the turbine heading direction) is different according to whether the load is applied from one side or the other. A single transformation matrix is needed for transverse loads (Fy) since the base is symmetrical in that direction.

2.2. Flow measurements

For performance assessment following IEC standards [17], two dedicated ADCP Measurement Campaigns (MC1 and MC2) were held. To measure incident current velocities, two Nortek Signature 500 ADCP were installed on the seabed between 50 and 60 m off turbine on each side, aligned with the main flow directions (Fig. 3). 'ADCP1' and 'ADCP2' refer to the instruments used during the first and the second measurement campaigns respectively. ADCPs noted '-NW' are used as the flood tide profilers and those noted '-SE' as the ebb tide profilers. Four acoustic beams are used to measure the current at 1 Hz in 0.5 m high cells on the whole water depth (varying from approximately 36 to 48 m between the Lowest and the Highest Astronomical Tide, noted LAT and HAT respectively). A fifth vertical beam is used to measure waves at 2 Hz in altimeter mode. The reference incident velocity (U_{cap}) is computed as the cubic power weighted average in time over 10 minutes and in space over the capture area (from $z =$ 5.2 m to 15.0 m above the seabed at the TEC position, assuming the velocity profile to be transversely homogeneous), as it is required in the IEC TS 62600-200 [17].

In addition, another Nortek Signature 500 ADCP, referred to as 'ADCP-HQ', fixed on the top of the turbine, measured the velocity profile (with 1 m cell size at 1 Hz) and the waves (at 2 Hz) above the turbine all the time during the 21 months of operation. Outside performance assessment campaigns, the data acquired by this instrument is used to qualify the sea state and to estimate the incident U_{cap}.

Apart from the power curve assessment that follows IEC TS 62600-200 [17], we study the data measured during the hour centred on the tidal velocity peak of each tidal cycle. The identification of this

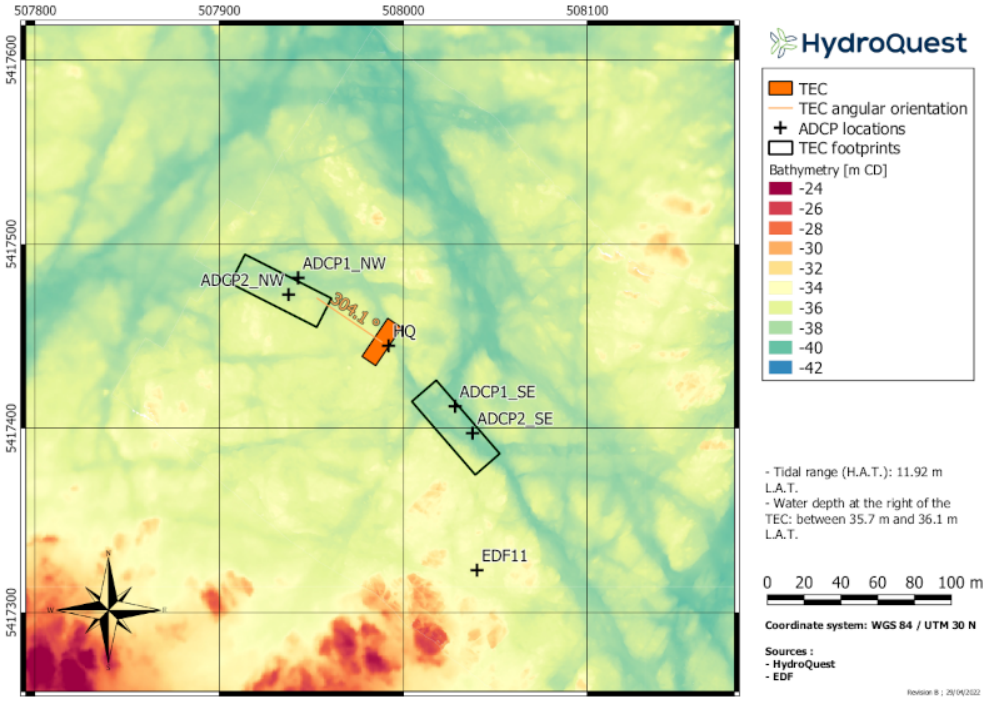

Figure 3: Acoustic Doppler Current Profilers (ADCP) positions around the turbine displayed on a bathymetry map. 'ADCP1' and 'ADCP2' refer to the instruments used during MC1 and MC2 respectively. The TEC footprints represent the areas, aligned with the main ebb and flood tide directions, in which the ADCPs must be placed for performance assessment according to the IEC TS 62600-200 [17].

instant is not straightforward since the velocity does not vary uniformly. To overcome this, we compute U_{cap} on the whole flood or ebb tidal cycle considered and fit the data with a third order polynomial which provides a single peak of velocity.

Finally, for spectral analysis, we compute the Fourier Transform (FT) of U_{HQ} which is the velocity measured by ADCP-HQ averaged in space over a surface equivalent to the capture area, approximately 5 meters above the turbine.

2.3. Flow characteristics

Fig. 4 illustrates the principal current directions relative to the TEC measured at the hub height during the first performance assessment campaign. The flood tide comes principally from the direction 297° and the principal ebb direction is 139°. Consequently, the misalignment between the TEC heading and the principal flood (resp. ebb) tide direction is equal to 7° (resp. 15°). The observed misalignments values are included in the domain defined by the design basis of the demonstrator. The flood tide current provides velocities with a maximum close to 3 m/s whereas the ebb current is lower, with a maximum around 2 m/s at the hub height.

10-minute averaged velocity profiles measured by the two ADCP1 in calm sea states are plotted on Fig. 5. We display the profiles measured within the two hours around the velocity peak, during three tidal cycles of range 6.2 m, 8.3 m and 10.5 m. The maximal tidal range between HAT and LAT being about 12 m, higher velocities can be expected during extreme tidal cycles. To have an idea of the average incident velocity profile, we first normalize each profile by its mean value over the capture area. Then, we plot the mean value of the normalized profiles at each altitude as well as the extreme values for ebb and flood tides on Fig. 6. The results show that the incident profile is almost self-similar between ebb and flood tides from the seabed to the top of the capture area of the turbine. Besides, we notice an important

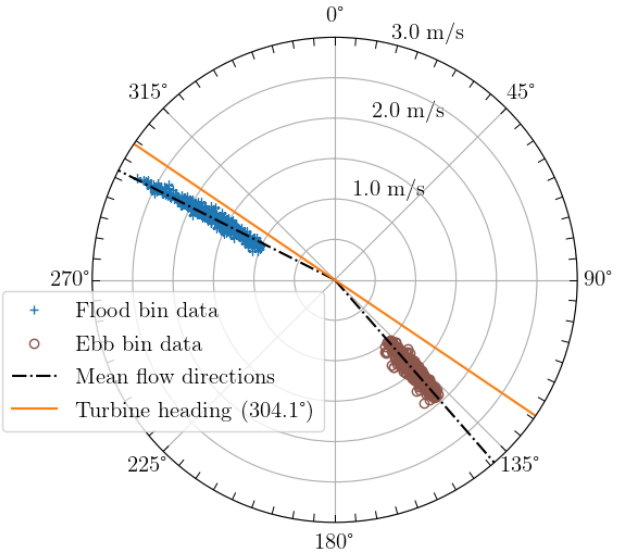

Figure 4: Tidal current magnitudes and origin directions at the hub height during MC1. Bin data refer to the method described in IEC TS 62600-200 [17].

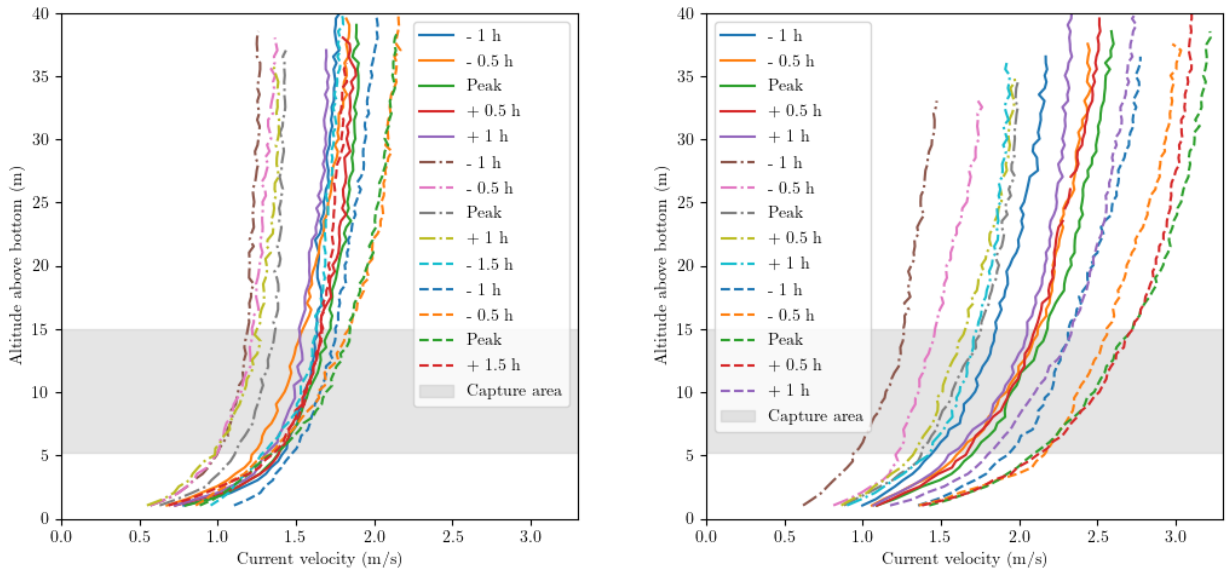

(a) Ebb tide

(b) Flood tide

Figure 5: Ebb and flood tide velocity profiles for three tidal ranges (-. 6.2 m, – 8.3 m, - - 10.5 m) at ± 1 h around the velocity peak, in calm sea conditions. The limit altitudes of the TEC's capture area are represented by the grey zone.

velocity shear at the altitude of the capture area with a 22 % (19 % resp.) velocity difference between the bottom and the top of the capture area for flood (ebb resp.) tide currents.

Concerning waves, the ADCP measurements reveal that the most important wave events over the test period are associated to swells coming from North-West (against ebb tide currents) with a peak period (Tp) of about 12 s (Fig. 7). The median significant wave height (Hs) computed on 30 minutes over this period is 1.15 m and the median Tp is 8.7 s. Besides, Hs remained below 1.7 m 75 % of the time. The

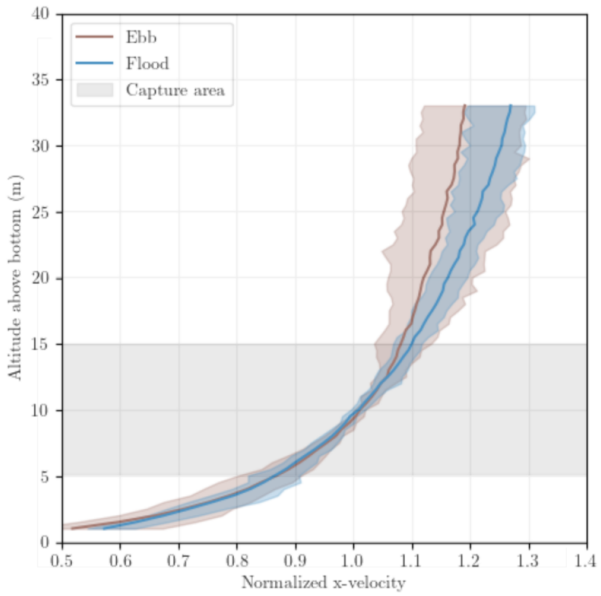

Figure 6: Statistical current velocity profiles calculated from the profiles on Fig. 5. The solid lines stand for the mean profiles and the shades for the range between minimal and maximal velocity values along the height. The statistical profiles are cut at z = 33 m to compute the mean over a constant number of profiles even though the water level varies.

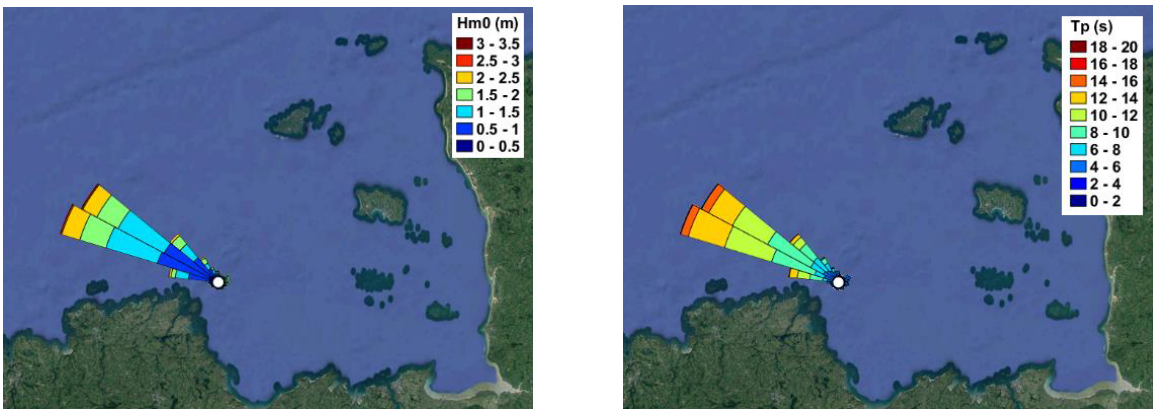

(a) Significant wave height

(b) Peak period

Figure 7: 30-minute wave statistics at Paimpol-Bréhat test site based on ADCP-IEC measurements from July to October 2019. NortekMED production.

most extreme wave event was measured in December 2019 with $Hs = 5.95$ m and $Tp = 11.9$ s but the TEC was parked to protect it from extreme loads.

Finally, EDF also performed an ADCP campaign at Paimpol-Bréhat test site in 2011. The ADCP was located at the position *EDF11* on the Fig. 3. From this campaign, the turbulent intensity at the turbine's height is evaluated around 15 % for current velocities over 1 m/s [22]. It is also showed that the turbulence decreases with the elevation in the water column and that it is higher during ebb tides than flood tides, probably due to the local bathymetry downstream and upstream the measurement point.

2.4. Data selection process

For the power curve assessment, according to the IEC TS 62600-200 [17], all the data acquired during the ADCP campaigns are considered, without sea state conditions discrimination.

For the wake consideration, the mechanical behaviour and loads analyses, we need to select specific instants representing the overall conditions to which the turbine was subjected among the 21 months of full time 1 Hz acquisition. As such, we developed an algorithm that helps identifying instants in specific conditions defined with criteria on the turbine status, the incident velocity and the wave conditions. In this paper, we focus on the instant at which the two columns of the turbine are in production mode during the hour centred on the tidal current velocity peak, both in flood and ebb tides, for a wide range of incident velocities. The wave conditions are differentiated into two categories: either *calm sea* with a significant wave height lower than 1.3 m and a peak period lower than 7 s or *rough sea* with Hs higher than 2 m and Tp higher than 10 s. With such criteria, the maximal orbital velocity expected at the top of the device according to Airy wave theory is less than 0.01 m/s in calm sea conditions and more than 0.30 m/s in rough sea.

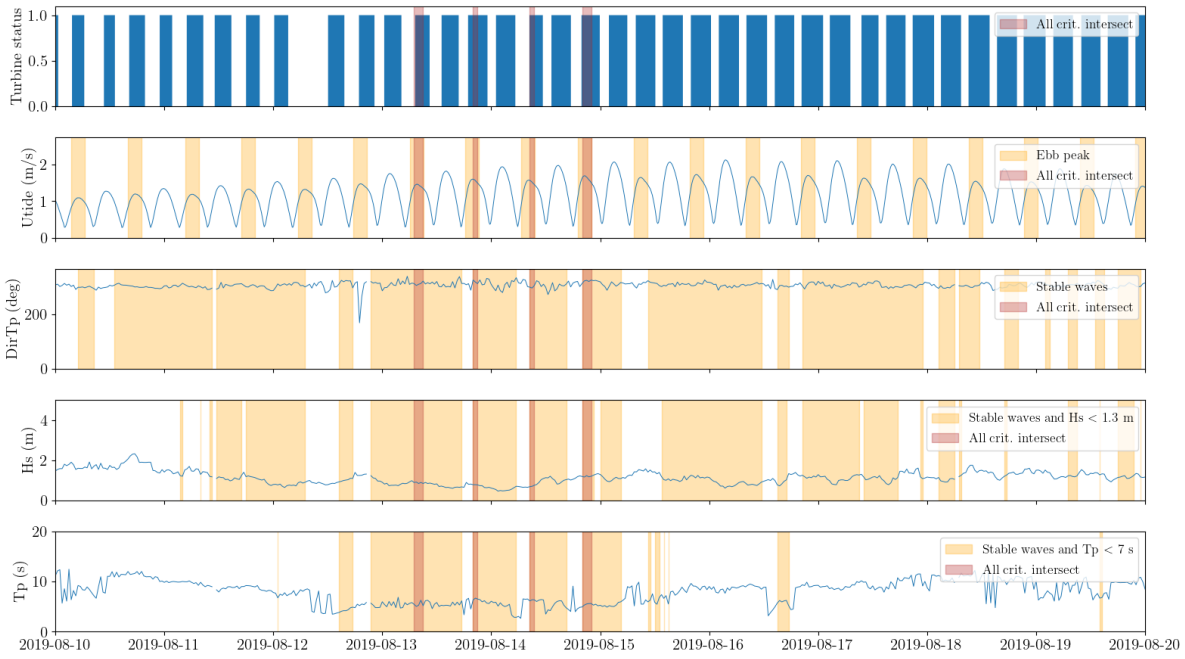

Figure 8: Illustration of the algorithm output for the selection of instants matching specific operating conditions and sea states. In this example, the conditions required are: turbine in production mode at ebb tide with calm wave conditions ($Hs < 1.3$ m and $Tp < 7$ s).

For the two categories, the wave conditions are established in terms of direction and peak period. Specifically, we select instants at which the waves direction varies less than 60° and the peak period less than 3 s during the 3 hours centred on those instants. An example of this algorithm's output is displayed in Fig. 8. Following this process, we identified about 40 moments matching the requested conditions on which the following mechanical behaviour and turbine wake studies are based.

3. Turbine performance and behaviour

In the following part, we analyse the performance and the behaviour of the turbine in the different sea states described above. The first section addresses an overview of the twin VATT power performance and wake. Then, the TEC behaviour is analysed in the temporal domain in terms of operating points and thrust, and in the spectral domain to highlight the periodic impact of waves on the machine. Finally, we discuss the impact of flow fluctuations on the mean and standard deviation of the TEC loads.

3.1. Overall analysis

3.1.1. Power curve assessment

Two measurement campaigns were held to assess the sensitivity of the power performance to the control parameter k. The 10-minute averaged active power generated by the TEC is plotted versus the mean power weighted tidal current velocity on Fig. 9 (a), following the IEC TS 62600-200 [17]. The results show that the ebb and flood tide power curves from MC1, when $k = 1.0$, are superimposed. This suggests that the turbine's performance is equivalent whether the flow comes from one side or the other of the machine and that the twin VATT is insensitive to flow misalignments with regard to its heading up to ± 15° (Fig. 4). However, this superimposition no longer observed during MC2, when $k = 1.5$, as the ebb power curve is lower than the flood power curve. Besides, it appears that the overall performance of the VATT is higher when $k = 1.5$ compared to $k = 1.0$ as the mean active power is 11 % and 36 % higher at ebb and flood tide, respectively, over the whole velocity range.

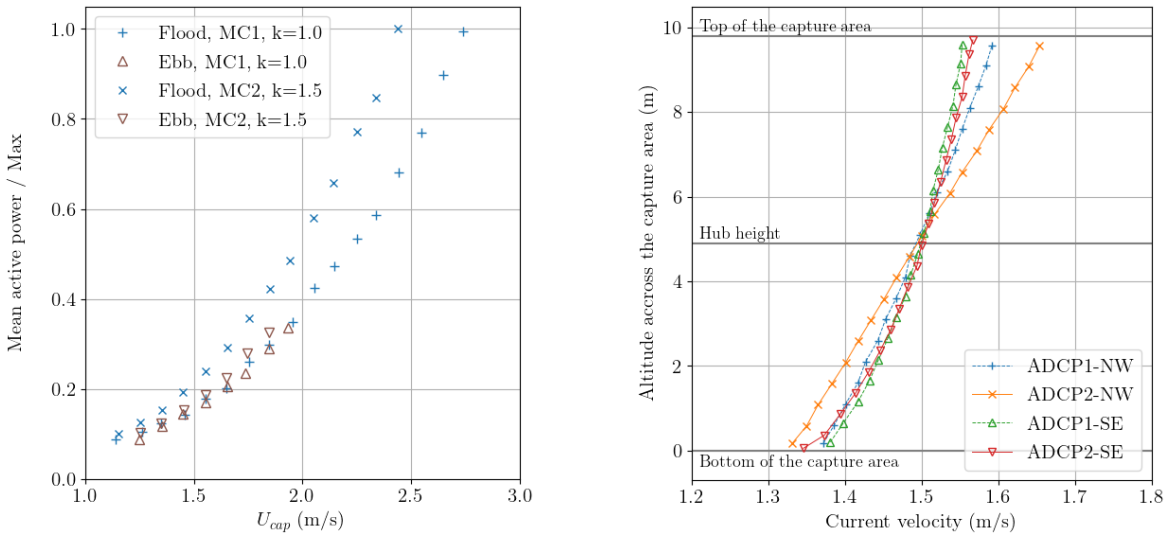

(a) Power curves

(b) Velocity profiles

Figure 9: (a) Power curves and (b) mean tidal current velocity vertical shear profiles when the mean velocity at the hub height is 1.5 ± 0.05 m/s, both established from MC1 and MC2 following the IEC TS 62600-200 method [17].

This performance improvement was expected since the control parameter value $k = 1.5$ had been adjusted to optimise the operating point of the turbine, but the flood performance increase exceeds the expectations. Beyond the tuning of k, the difference between MC1 and MC2 curves are also probably due, in part, to the change in the ADCP locations between the two campaigns, even if the IEC standards are respected (Fig. 3). Indeed, the measured flow characteristics, such as turbulence and velocity profile, depend strongly on the instruments position downstream bathymetric variations [30]. Fig. 9 (b) presents the mean tidal current velocity vertical shear profiles during MC1 and MC2 when the mean velocity at the hub height is 1.5 ± 0.05 m/s, as defined in the IEC TS 62600-200 [17]. The flood profiles (ADCPs -NW) are significantly different between the two campaigns, showing the spatial variability of the flow. Since the computation of U_{cap} is based on the assumption that the velocity profile is homogeneous over the turbine width, there is an uncertainty on its value that can explain part of the difference between MC1 and MC2 power curves. The TEC footprints where the ADCP can be installed, as defined in the IEC standards and represented in Fig. 3, should be narrowed to make the flow measurements, and thus the performance assessments, more comparable between different measurement campaigns.

3.1.2. Wake consideration

For power curve assessment, only the upstream ADCP is considered in the process. Hereafter, we propose to analyse the downstream ADCP measurements to study the TEC wake characteristics in calm sea states. The velocity deficit observed during ebb tides by the ADCP2-NW (Fig. 11 (a & b)) extends from the bottom of the capture area of the turbine up to 5 meters above it and represent 15 to 20 % of the incident velocity at its maximum, in the top half of the capture area. We can also observe an over-speed between the seabed and the bottom of the turbine indicating that the incident flow tries to bypass the obstacle. This velocity profile shape is similar to the one computed numerically by Grondeau et al. [28].

As shown in Fig. 10, the instruments are placed approximately 55 m on each side of the turbine, being about 2.2 times the TEC width (W). However, the downstream ADCPs are not properly aligned with the main incident flow direction and the TEC due to the asymmetry between flood and ebb tides (Fig. 4). Fig. 10 displays the ADCP locations with regard to the TEC boundaries projections along the main ebb and flood tide directions. It shows that the two ADCP1 are located on the edge of the projections downstream of the TEC and that the two ADCP2 are outside these projections.

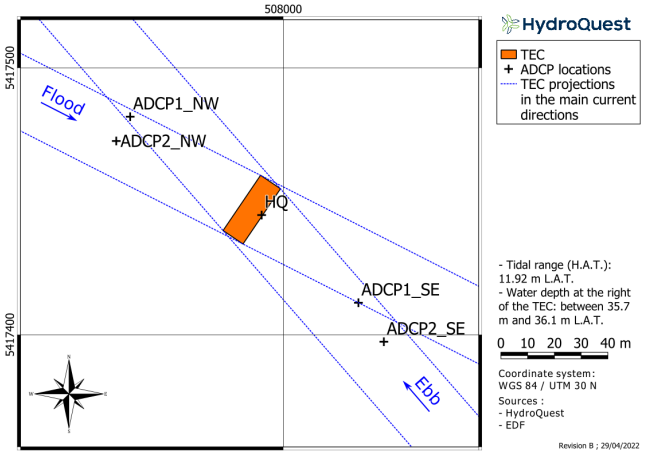

Figure 10: ADCP locations with regard to the TEC boundaries projections along the main ebb and flood tide directions.

Numerically, the wake almost hardly expands laterally and remains within the TEC projection along the flow direction at $2W$ downstream distance [28, 31]. Consequently, it is not surprising to observe that the ADCP2-SE does not measure any velocity deficit at flood tide (Fig. 11 (c)), which shows that it is outside the wake region. However, even though the upstream profile data is lacking for a proper comparison, we can clearly see a velocity deficit at the turbine height in the ADCP1-SE measurement, located downstream at flood tides (Fig. 11 (d)). These observations suggest that the wake lateral boundary is located between the two instrument positions, which is coherent with the numerical simulation results [28, 31].

During ebb tides (Fig. 11 (a and b)), the ADCP2-NW measures a clear velocity deficit even though it is located outside the TEC projection, unlike the ADCP2-SE at flood tide. The difference of wake behaviour between ebb and flood tides can be explained by different hypotheses. Firstly, the 2D numerical simulation of *OceanQuest* presented in [31] shows that the wake expands a bit more laterally when the turbine operates in WFI counter-rotating configuration, as at ebb tide, than in AFI, as at flood tide. Secondly, the lateral fairings of the turbine probably guide the flow along its own heading, diverting the wake from the flow's incident direction. We assume that the wake remains diverted from the incident direction further downstream at ebb tide than at flood tide as the incident velocity magnitude is lower at ebb tide. This flow behaviour was not predicted numerically in [31] but the numerical model had been validated by comparison to a single vertical axis rotor, without surrounding fairing. Consequently, it

appears that a more complete characterisation of the TEC wake, either in-situ or at least experimentally, is required both to better understand its physics and to validate numerical models.

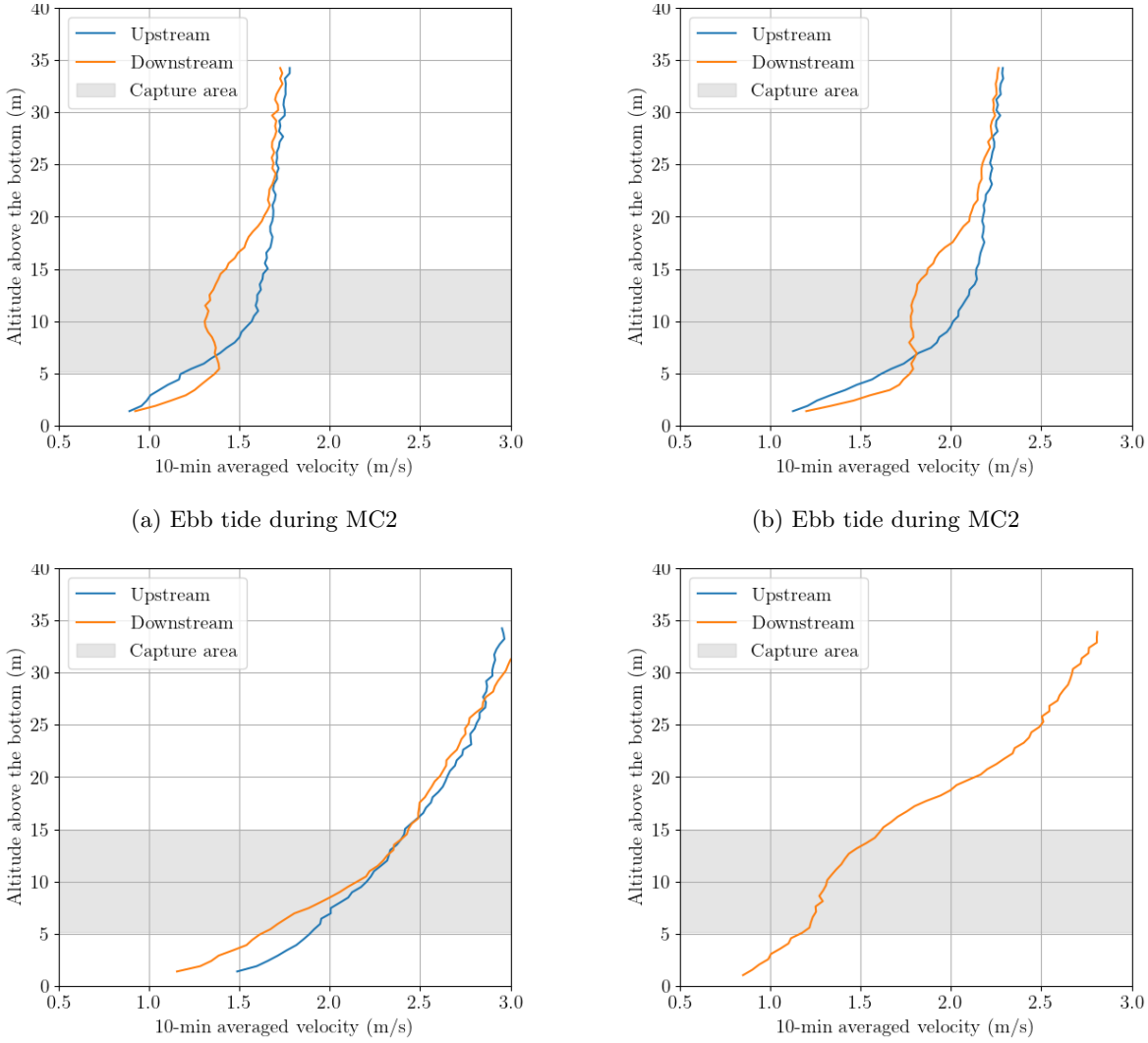

(a) Ebb tide during MC2

(b) Ebb tide during MC2

(c) Flood tide during MC2

(d) Flood tide during MC1

Figure 11: Upstream and downstream 10-minutes averaged velocity profiles at the tidal velocity peak measured by bottom mounted ADCP placed as shown in Fig. 3, with the turbine is in production mode.

3.2. Mechanical behaviour investigation

To go into the demonstrator characterisation in depth, specific developments are carried out to analyse the 1 Hz signals in the temporal and spectral domains as well as their statistics. To focus on the influence of sea states on the VATT and avoid discussions on the control law effects, we consider only the data points corresponding to a single control parameter value ($k = 1.0$).

3.2.1. Temporal domain

Fig. 12 presents a time series at 1 Hz of the axial load on the turbine during the hour centred on the tidal velocity peak. Fig. 12 (a and b) are at flood tide with a similar incident velocity of approximately 2.1 m/s, in calm and rough sea conditions respectively, and Fig. 12 (c and d) are at ebb tide with a

similar incident velocity of approximately 1.5 m/s, in calm and rough sea conditions respectively too. As explained in the section 2.1, two transformation matrixes, using different strain gauges, are needed to assess axial loads in the two directions (positive or negative) due to the base asymmetry. For equivalence between flood and ebb tide, Fig. 12 displays the absolute value of the axial load in the main direction (Fx) and its opposite ($Fx - opp$) in negative. From these plots, it is obvious that the presence of harsh waves generates significantly stronger fluctuations in the axial load, without shifting significantly the mean value for similar incident velocity. Besides, one can notice on Fig. 12 (d) that when the mean velocity is low, and so the mean Fx load too, the waves generate loads in the direction opposed to the current flow direction. However, given the instrumentation used, we cannot fully recompose the time series of the loads when its sign changes. Consequently, for the analysis of the turbine's behaviour that follows, only the Fx signals are considered.

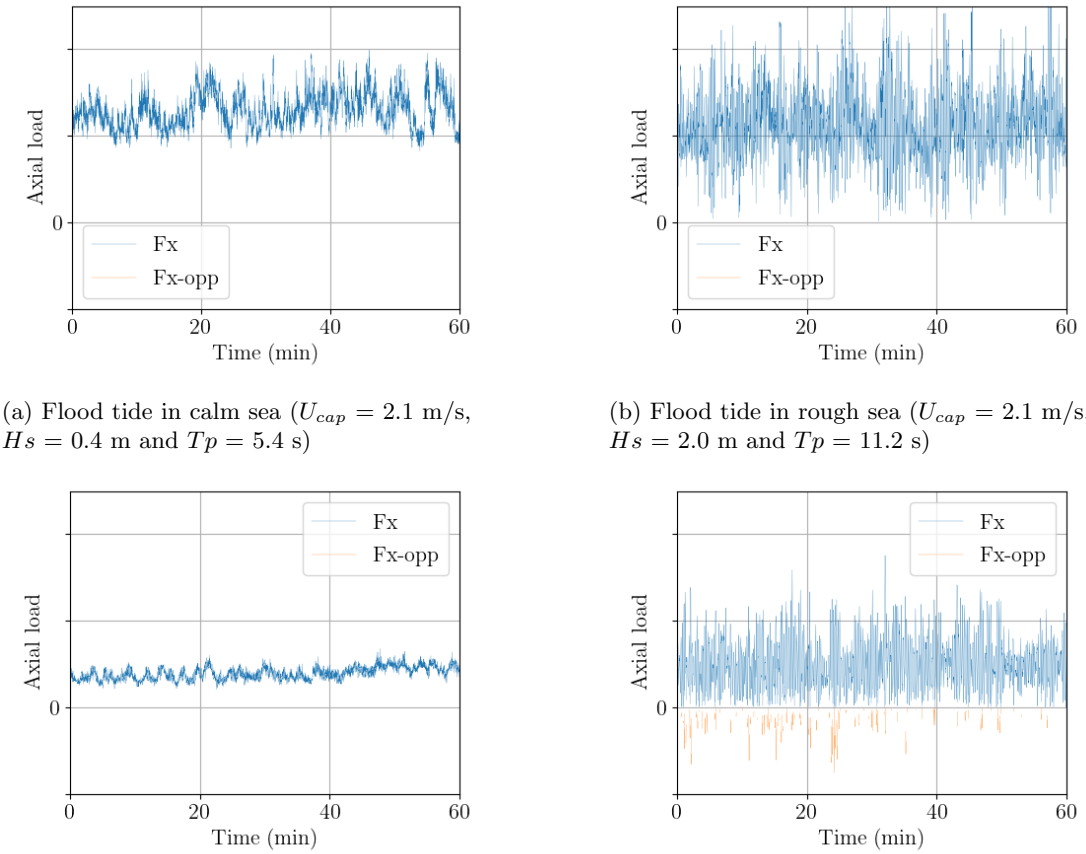

(a) Flood tide in calm sea (U_{cap} = 2.1 m/s, Hs = 0.4 m and Tp = 5.4 s)

(b) Flood tide in rough sea (U_{cap} = 2.1 m/s, Hs = 2.0 m and Tp = 11.2 s)

(c) Ebb tide in calm sea (U_{cap} = 1.5 m/s, Hs = 1.2 m and Tp = 5.3 s)

(d) Ebb tide in rough sea (U_{cap} = 1.5 m/s, Hs = 3.0 m and Tp = 11.7 s)

Figure 12: Time series of the axial load on the turbine during the hour centred on the peak tidal velocity of each tidal cycle. Fx is the axial load computed from the strain gauges with the transformation matrix defined for loads in the current direction considered and $Fx - opp$ is the measurement using the transformation matrix defined for the opposite direction. The vertical axis scale is the same for the four plots but the values are not communicated.

To complete the mechanical behaviour analysis of the demonstrator, Fig. 13 displays the operating points of the two generators at 1 Hz during the hour centred on the tidal velocity peak in six different situations. The control law of the generators, displayed in black lines, is based on two curves: one that applies a torque (Q) proportional to the rotational speed (ω) to the square (Eq. 2) and one limiting the output power to a maximal value by speeding (Eq. 3). Consequently, when the incident velocity increases

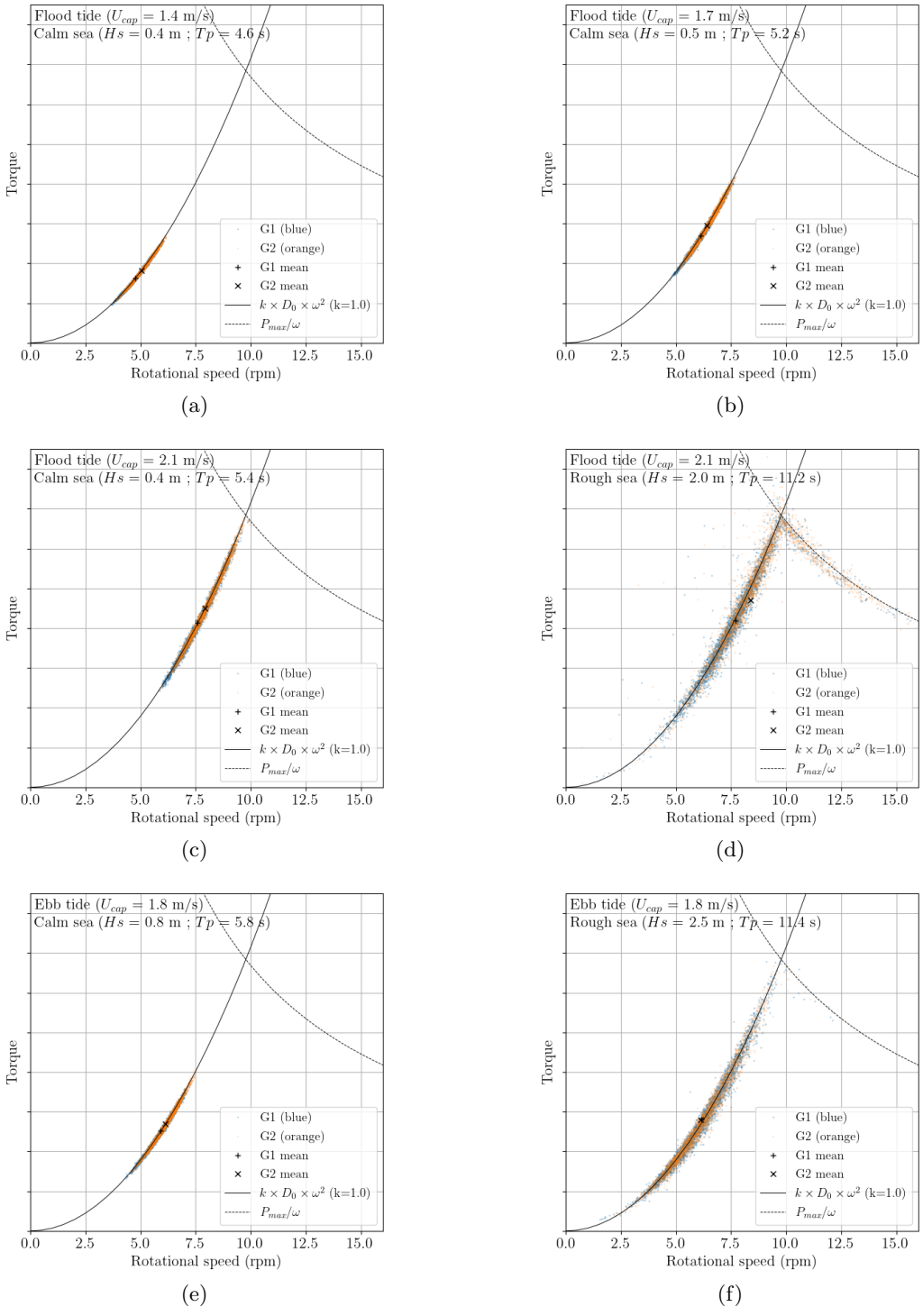

Figure 13: Operating point of the two generators (G1 in blue, G2 in orange) at 1 Hz over the hour centred on the peak tidal velocity. (a, b & c) are at flood tide in calm sea conditions with $U_{cap} = \{1.4, 1.7, 2.1\}$ m/s respectively. (c & d) are at flood tide with $U_{cap} = 2.1$ m/s in calm and rough sea states respectively. (e & f) are at ebb tide with $U_{cap} = 1.8$ m/s in calm and rough sea states respectively. The black crosses represent the mean operating point and the black lines the control laws. The vertical axis scale is the same for the six plots but the values are not communicated.

in calm sea conditions (Fig. 13 a, b and c), the mean operating point (indicated by the black crosses) shifts to higher Q and ω. In addition, it appears that the spreading of the operating points along the control law curve increases with the mean operating point. Furthermore, by comparing Fig. 13 c and e to d and f respectively, one can see that the presence of important surface waves increases the operating point fluctuations significantly even if the mean incident velocity U_{cap} is constant. When the latter is high, the presence of waves can even lead the generators to operate following the power limiting control law while this is not the case in calm sea conditions (Fig. 13 c and d). Conversely, the mean operating point over the hour are unchanged between rough and calm sea conditions, given the uncertainty on the mean incident velocity assessment, when the power limit is not reached.

3.2.2. Spectral domain

For spectral analysis of the mechanical behaviour we focus on two pairs of cases with high incident current velocity, corresponding to the cases presented in Fig. 13 (c to f), to avoid uncertainties due to sign changes in the axial load for the spectral analysis (Section 3.2.1). Fig. 14 compares the spectral response of the demonstrator at flood (a and b) and ebb tides (c and d), in calm (a and c) and rough sea states (b and d). Each sub-figure presents the Fourier Transform (FT) of the velocity measured above the turbine and averaged on a surface equal to the capture area (U_{HQ}), the FT of the torque of the two generators (Q_{G1} and Q_{G2}) and of the axial and transverse loads. In addition, the bottom subplot displays the coherence function between the velocity and the torque as well as between the velocity and the axial load spectra.

On one hand, in the case of calm sea states, the frequency content of the turbine response and of the flow is poor with most of the response contained mainly in the low frequencies, below 0.06 Hz, and without any peaks at higher frequencies. Consequently, the coherence function of the velocity with the torque and with the axial load is below 0.5 at all the frequencies meaning that the turbine response is not related to the flow fluctuations. Besides, a peak related to the blade passing frequency is expected [11] but the Nyquist frequency of these 1 Hz measurement is too low to observe it.

On the other hand, in rough sea states, the velocity FT shows the contribution of the waves to the flow fluctuations, between 0.05 and 0.2 Hz. The pattern observed on the velocity FT is easily recognisable on the torque and loads FT, which is confirmed by the high levels of coherence between the spectra. One can also notice that the coherence level is at its maximum for the lowest frequency waves and decreases as the frequency increases. This shows that the demonstrator responds more strongly to long period waves. Overall, this result reveals the high sensitivity of the bottom mounted twin VATT to the periodic loads induced by surface waves.

3.3. Loads statistics

This last section aims at summarising the sea states influence on the VATT response by studying most of the instants identified using the algorithm described in the Section 2.4 from a statistical point of view. Given the fact that the two rotor columns behave similarly both in the temporal and spectral domain, the following analysis focuses on the generator 1.

Fig. 15 displays the normalised average over the hour centred on the tidal velocity peak of the rotational speed, the torque and the axial load for the calm and rough sea states, with regard to the incident velocity. The three quantities increase along the same trend whether in calm or rough sea states when U_{cap} increases, showing the insensitivity of the VATT to the sea states in average. The torque and thrust averages increase faster with U_{cap} as they depend on the flow velocity to the power two while the rotational speed depends on the velocity to the power one.

Besides, to quantify the load fluctuations induced by the flow, Fig. 16 presents the Fluctuation Intensity (FI, standard deviation divided by mean) of the rotational speed, the torque and the axial load for the calm and rough sea states. It appears that in calm sea state, the FI of the rotational speed, the

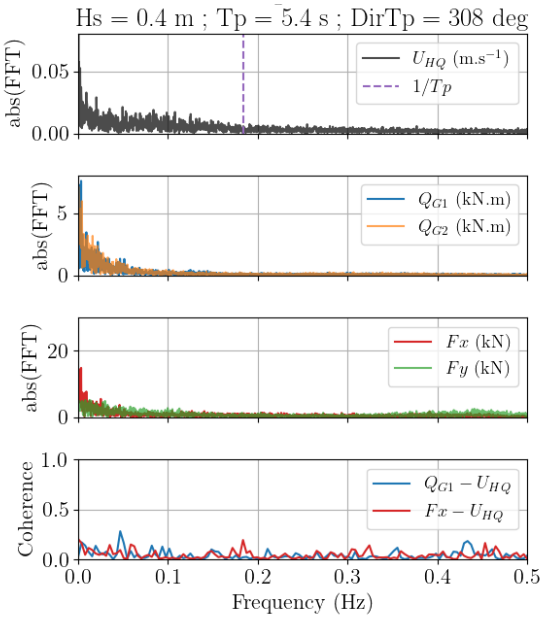

(a) Flood tide in calm sea (U_{cap} = 2.1 m/s)

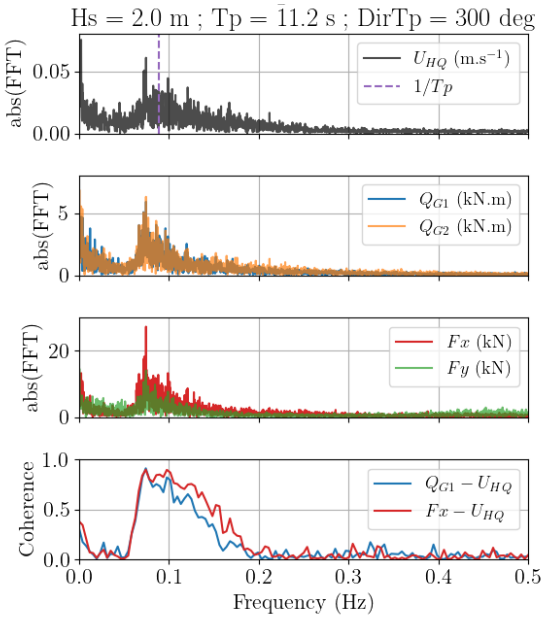

(b) Flood tide in rough sea (U_{cap} = 2.1 m/s)

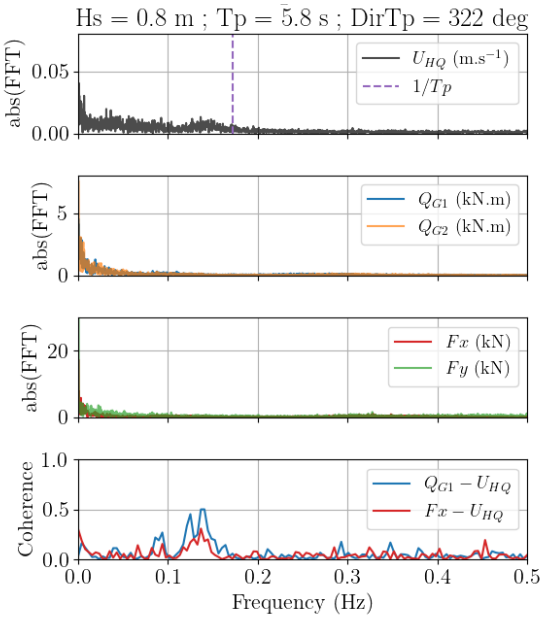

(c) Ebb tide in calm sea (U_{cap} = 1.8 m/s)

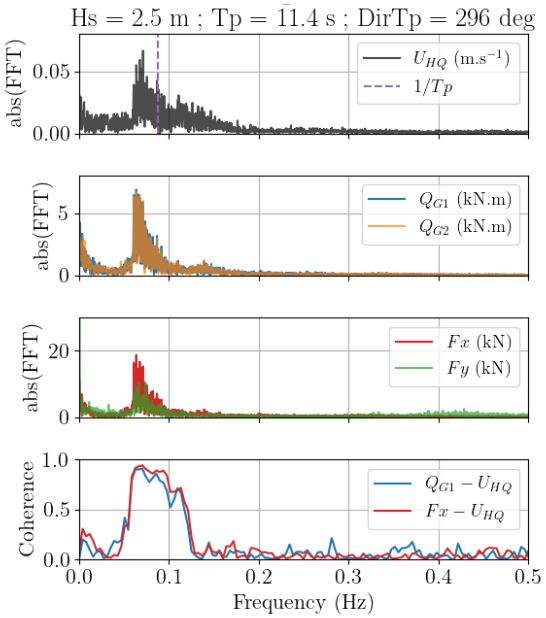

(d) Ebb tide in rough sea (U_{cap} = 1.8 m/s)

Figure 14: Each sub-figure presents the Fourrier Transform of the torques of each generator (Q_{G1} and Q_{G2}), of the axial and transverse loads and of the vertically averaged velocity measured above the turbine (U_{HQ}) as well as the coherence function between $Q_{G1} - U_{HQ}$ and $Fx - U_{HQ}$. Cases on the left are in calm sea states and in rough sea states on the right, at flood tide at the top and ebb tide at the bottom. The data analysed is the hour centred on the peak velocity.

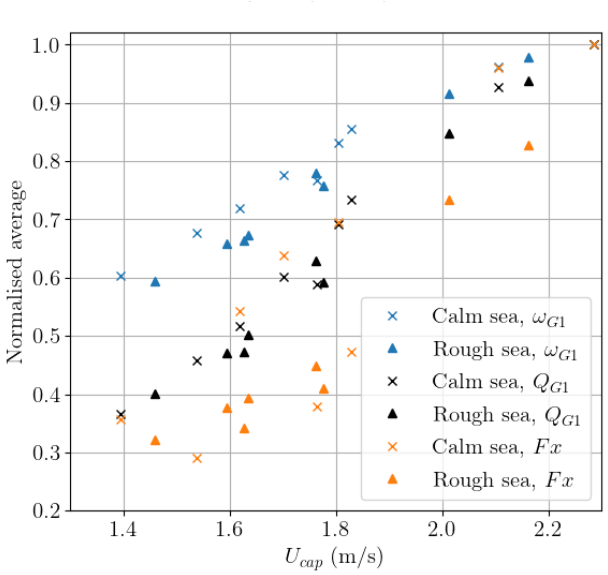

Figure 15: Normalised average over the hour centred on the tidal velocity peak of the torque (C_{G1}) and the rotational speed (ω_{G1}) of the generator 1, and of the axial load (Fx) with regard to U_{cap}. Each quantity is normalised by its maximal value.

torque and the axial load are insensitive to the incident velocity magnitude. In average over the points in calm sea, FI is 9.0 % for ω_{G1}, 17.9 % for C_{G1} and 16.1 % for Fx. This trend with regard to the velocity magnitude is like the turbulence intensity, which is the FI of the velocity. For a constant tip speed ratio ($\omega R/U$), the rotational speed is proportional to the incident velocity. However, the turbulence intensity is assessed between 15 and 20 % at Paimpol-Bréhat test site [22], which is about two times $FI(\omega_{G1})$. Consequently, it means that the VATT is not sensitive to all the flow fluctuations induced by turbulence. The blades are very likely not sensitive to turbulent structures of a small length scale compared to their own geometry. We assume that the turbine behaves as a low-pass filter between the flow fluctuations and the rotational speed (and so the torque) fluctuations as it is observed at lab-scale. Indeed, Deskos et al. [32] show that the power spectra of a lab-scale horizontal axis tidal turbine follows the velocity spectra behaviour in the large turbulent scales region but has a steeper slope behaviour over the inertial frequency sub-range, illustrating the low-pass filtering of the turbine.

Furthermore, the average FI in rough sea states over the whole velocity range appear to be 3.0 times higher for ω_{G1}, 2.7 for C_{G1} and 3.1 for Fx compared to the calm sea state. The torque and thrust FI exceed 50 % when Hs is higher than 2.8 m, reaching almost 70 % for the largest waves (Hs ; Tp) $\simeq$ (3.1 m ; 14 s). One can also notice that the machine loads FI in rough sea states decrease with U_{cap}. The first explanation for this result is the definition of FI itself, which is the division of the standard deviation by the average of the signal. A given wave induces a given periodic solicitation and so a given standard deviation of the loads. Besides, the average of the three quantities considered increases with U_{cap} (Fig. 15). Consequently, for a given wave, the ratio of the loads standard deviation to the average decreases when the velocity increases. A second explanation, due to a database bias, intensifies this trend. Indeed, Fig. 16 (b) shows that the FI increases with Hs and Tp. But, by putting Fig. 16 (a) and (b) together, it appears that the cases at high Hs are also those at low U_{cap}, and vice versa. Thus, even though the database is made of 21 months of measurements, it does not allow us to decorrelate clearly the influence of the incident velocity and the waves height on the evolution of FI in rough sea states.

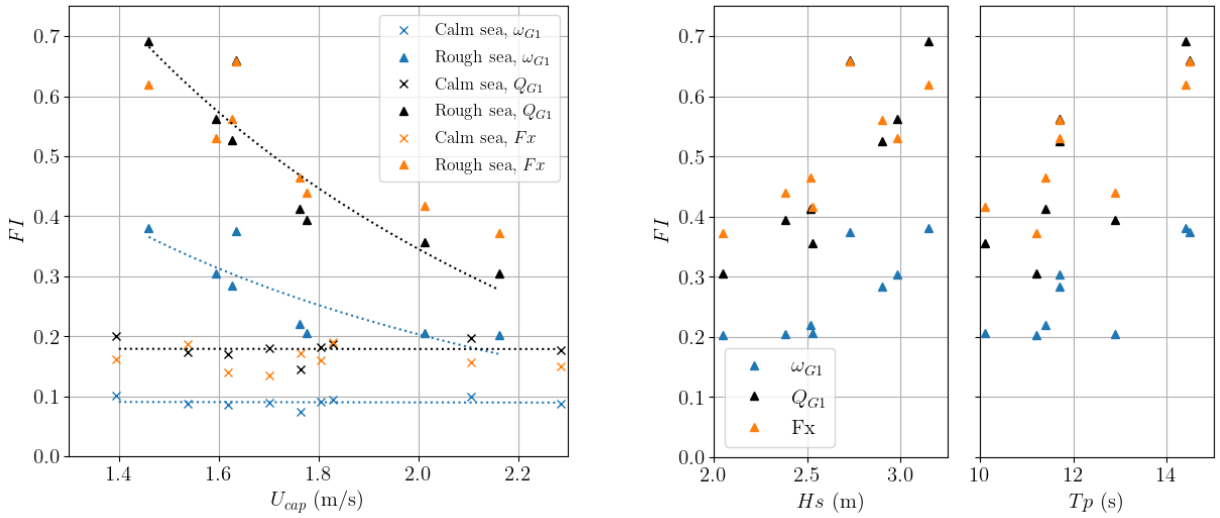

(a) (b)

Figure 16: (a) Fluctuation intensities (FI) over the hour centred on the tidal velocity peak of C_{G1}, ω_{G1} and Fx with regard to U_{cap}. (b) Fluctuation intensities of Fx and ω_{G1} in rough sea states with regard to the wave parameters Hs and Tp.

4. Conclusions

HydroQuest achieved full scale deployment in spring 2019 when it immersed its first 1 MW capacity tidal turbine at EDF's Paimpol-Bréhat test site. More than two years after its immersion, the machine was retrieved, although still fully operational, showing the reliability of such bottom mounted twin vertical axis turbines. The demonstrator was equipped with instrumentation to measure electrical power generation, rotors rotational speed and turbine loads. Acoustic Doppler Current Profilers were also placed around the turbine to qualify the incident flow velocity profiles and the surface waves characteristics.

The characterisation of the environmental conditions present at Paimpol-Bréhat show that the ebb and flood tide directions are not symmetrical, leading to a turbine misalignment of about 7° at flood and 15° at ebb tide, and that the velocity profile is strongly sheared at the turbine height. Surface waves appear to propagate mainly in the same direction as flood tide and are, therefore, mainly against ebb tide currents.

The mechanical behaviour analysis shows that the presence of surface waves multiplies the fluctuation intensities of rotational speed, torque and thrust by almost 3 compared to cases in calm sea state. The latter exceeds 50 % for thrust and torque when Hs is higher than 2.8 m and reaches 70 % for the largest waves (Hs ; Tp) $\simeq$ (3.1 m ; 14 s), without shifting significantly the average values. This fluctuation increase appears to be directly linked to the periodic solicitations of the waves in the spectral domain, even though the demonstrator is installed more than 35 m below the surface. We also observed that the fluctuation intensity of the rotational speed is about 2 times lower than the turbulence intensity, which shows that the turbine behaves as a low-pass filter, whatever the control parameter.

To complete this study, a better characterisation of the spatial variability of the flow and of the influence of the ADCP position on the mean incident velocity assessment would help explaining the power curve differences. In addition, proper wake measurement campaigns would be needed to complete its characterisation and to explain why the turbine wake behaves differently between ebb and flood tides. Finally, in a near future, these results will be compared to those obtained at lab-scale to characterise scale effects and define proper extrapolation laws from reduced scale results to full scale.

Acknowledgement

This work was supported in part by ANRT under convention Cifre n°2020/0688 and by ADEME in the framework of the OCEANQUEST project.

References

[1] P. Mycek, B. Gaurier, G. Germain, G. Pinon, and E. Rivoalen, "Experimental study of the turbulence intensity effects on marine current turbines behaviour. Part I: One single turbine," *Renewable Energy*, vol. 66, pp. 729–746, 2014. [Online]. Available: http://dx.doi.org/10.1016/j.renene.2013.12.036

[2] T. Ebdon, M. J. Allmark, D. M. O'Doherty, A. Mason-Jones, T. O'Doherty, G. Germain, and B. Gaurier, "The impact of turbulence and turbine operating condition on the wakes of tidal turbines," *Renewable Energy*, vol. 165, pp. 96–116, mar 2021. [Online]. Available: https://doi.org/10.1016/j.renene.2020.11.065

[3] G. S. Payne, T. Stallard, R. Martinez, and T. Bruce, "Variation of loads on a three-bladed horizontal axis tidal turbine with frequency and blade position," *Journal of Fluids and Structures*, vol. 83, no. 2018, pp. 156–170, 2018. [Online]. Available: https://doi.org/10.1016/j.jfluidstructs.2018.08.010

[4] L. Chatellier, J. Gorle, F. Pons, and B. Malick, *Towing tank testing of a controlled-circulation Darrieus turbine*. Lisbon, Portugal: CRC Press, oct 2018. [Online]. Available: https://www.taylorfrancis.com/books/9780429505324

[5] S. Hoerner, C. Bonamy, O. Cleynen, T. Maître, and D. Thévenin, "Darrieus vertical-axis water turbines: deformation and force measurements on bioinspired highly flexible blade profiles," *Experiments in Fluids*, vol. 61, no. 6, pp. 1–17, 2020. [Online]. Available: https://doi.org/10.1007/s00348-020-02970-2

[6] L. Priegue and T. Stoesser, "The influence of blade roughness on the performance of a vertical axis tidal turbine," *International Journal of Marine Energy*, vol. 17, pp. 136–146, 2017. [Online]. Available: http://dx.doi.org/10.1016/j.ijome.2017.01.009

[7] B. Gaurier, S. Ordonez-Sanchez, J.-V. Facq, G. Germain, C. Johnstone, R. Martinez, F. Salvatore, I. Santic, T. Davey, C. Old, and B. Sellar, "MaRINET2 Tidal Energy Round Robin Tests—Performance Comparison of a Horizontal Axis Turbine Subjected to Combined Wave and Current Conditions," *Journal of Marine Science and Engineering*, vol. 8, no. 6, p. 463, jun 2020. [Online]. Available: https://doi.org/10.3390/jmse8060463

[8] S. Draycott, A. Nambiar, B. Sellar, T. Davey, and V. Venugopal, "Assessing extreme loads on a tidal turbine using focused wave groups in energetic currents," *Renewable Energy*, vol. 135, pp. 1013–1024, 2019. [Online]. Available: https://doi.org/10.1016/j.renene.2018.12.075

[9] P. Druault, B. Gaurier, and G. Germain, "Spatial integration effect on velocity spectrum: Towards an interpretation of the -11/3 power law observed in the spectra of turbine outputs," *Renewable Energy*, vol. 181, pp. 1062–1080, jan 2022. [Online]. Available: https://doi.org/10.1016/j.renene.2021.09.106

[10] M. Moreau, G. Germain, G. Maurice, A. Richard, and R. Coquet, "HydroQuest : Feedback from Paimpol-Bréhat and validation of the design method," in *14th European Wave and Tidal Energy Conference*, Plymouth, 2021, pp. 2229–1—-8.

[11] M. Harrold and P. Ouro, "Rotor Loading Characteristics of a Full-Scale Tidal Turbine," *Energies*, vol. 12, no. 6, p. 1035, mar 2019. [Online]. Available: https://doi.org/10.3390/en12061035

[12] G. T. Scarlett, B. Sellar, T. van den Bremer, and I. M. Viola, "Unsteady hydrodynamics of a full-scale tidal turbine operating in large wave conditions," *Renewable Energy*, vol. 143, no. March 2020, pp. 199–213, 2019. [Online]. Available: https://doi.org/10.1016/j.renene.2019.04.123

[13] Black & Veatch, "Lessons Learnt from MeyGen Phase 1A Final Summary Report," Black & Veatch Corporation, Tech. Rep., 2020. [Online]. Available: https://h7g7q8k5.stackpathcdn.com/cdn/ff/Yysz2k-kjIRKTcXlXt-xYQfAqKSp3t2ZYxpB4f17pTE/1593113924/public/2020-06/MeyGenLessonsLearntFullReport.pdf

[14] Z. Goss, D. Coles, and M. Piggott, "Economic analysis of tidal stream turbine arrays: a review," pp. 1–29, 2021. [Online]. Available: http://arxiv.org/abs/2105.04718

[15] P. Jeffcoate, R. Starzmann, B. Elsaesser, S. Scholl, and S. Bischoff, "Field measurements of a full scale tidal turbine," *International Journal of Marine Energy*, vol. 12, no. 2015, pp. 3–20, 2015. [Online]. Available: https://doi.org/10.1016/j.ijome.2015.04.002

[16] D. Coles, A. Angeloudis, D. Greaves, G. Hastie, M. Lewis, L. Mackie, J. McNaughton, J. Miles, S. Neill, M. Piggott, D. Risch, B. Scott, C. Sparling, T. Stallard, P. Thies, S. Walker, D. White, R. Willden, and B. Williamson, "A review of the UK and British Channel Islands practical tidal stream energy resource," *Proceedings of the Royal Society A: Mathematical, Physical and Engineering Sciences*, vol. 477, no. 2255, nov 2021. [Online]. Available: https://doi.org/10.1098/rspa.2021.0469

[17] IEC TS 62600-200, "International electrotechnical commission, technical specification 62600-200: Electricity producing tidal energy converters – power performance assessment," in *Marine energy – Wave, tidal and other water current converters*, 2013.

[18] U. Rathnayake, M. Folley, S. D. Gunawardane, and C. Frost, "Investigation of the error of mean representative current velocity based on the method of bins for tidal turbines using ADP data," *Journal of Marine Science and Engineering*, vol. 8, no. 6, p. 390, jun 2020. [Online]. Available: http://doi.org/10.3390/JMSE8060390

[19] M. Guerra and J. Thomson, "Turbulence Measurements from Five-Beam Acoustic Doppler Current Profilers," *Journal of Atmospheric and Oceanic Technology*, vol. 34, no. 6, pp. 1267–1284, jun 2017. [Online]. Available: https://doi.org/10.1175/JTECH-D-16-0148.1

[20] A. Bouferrouk, J. B. Saulnier, G. H. Smith, and L. Johanning, "Field measurements of surface waves using a 5-beam ADCP," *Ocean Engineering*, vol. 112, pp. 173–184, 2016. [Online]. Available: http://dx.doi.org/10.1016/j.oceaneng.2015.12.025

[21] M. Togneri, I. Masters, A. Williams, and I. Fairley, "A spectral-statistical filter for decoupling wave and turbulence effects at tidal sites," *Proceedings of the European Wave and Tidal Energy Conference*, pp. 1927–1—-10, 2021.

[22] J.-F. Filipot, M. Prevosto, C. Maisondieu, M. Le Boulluec, and J. Thomson, "Wave and turbulence measurements at a tidal energy site," in *IEEE/OES 11th Current, Waves and Turbulence Measurement (CWTM)*, 2015, pp. 1–9. [Online]. Available: http://doi.org/10.1109/CWTM.2015.7098128

[23] P. Mercier, M. Thiébaut, S. Guillou, C. Maisondieu, E. Poizot, A. Pieterse, J. Thiébot, J. F. Filipot, and M. Grondeau, "Turbulence measurements: An assessment of Acoustic Doppler Current Profiler accuracy in rough environment," *Ocean Engineering*, vol. 226, no. December 2020, p. 108819, 2021. [Online]. Available: https://doi.org/10.1016/j.oceaneng.2021.108819

[24] L. Terme and N. Gerard, "Parc hydrolien EDF de Paimpol-Bréhat : premières réalisations et préparation du raccordement au réseau de la première ferme hydrolienne en France," *La Houille Blanche*, no. 1, pp. 22–26, feb 2015. [Online]. Available: https://doi.org/10.1051/lhb/2015003

[25] C.-T. Pham and V. a. Martin, "Tidal current turbine demonstration farm in Paimpol-Brehat (Brittany): tidal characterisation and energy yield evaluation with Telemac," *Proceedings of the 8th European Wave and Tidal Energy Conference*, pp. 181–188, 2009.

[26] C.-T. Pham and K. Pinte, "Paimpol-Bréhat tidal turbine demonstration farm (Brittany): optimisation of the layout , wake effects and energy yield evaluation using Telemac," *International Conference on Ocean Energy*, 2010.

[27] J.-L. Achard and T. Maître, "Hydraulic turbomachine," 2006. [Online]. Available: https://hal.archives-ouvertes.fr/hal-00189351

[28] M. Grondeau, S. Guillou, P. Mercier, and E. Poizot, "Wake of a ducted vertical axis tidal turbine in turbulent flows, LBM actuator-line approach," *Energies*, vol. 12, no. 22, p. 4273, nov 2019. [Online]. Available: https://doi.org/10.3390/en12224273

[29] N. Guillaud, G. Balarac, E. Goncalvès, and J. Zanette, "Large eddy simulations on vertical axis hydrokinetic turbines - Power coefficient analysis for various solidities," *Renewable Energy*, vol. 147, pp. 473–486, mar 2020. [Online]. Available: https://doi.org/10.1016/j.renene.2019.08.039

[30] M. Ikhennicheu, G. Germain, P. Druault, and B. Gaurier, "Experimental investigation of the turbulent wake past real seabed elements for velocity variations characterization in the water column." *International Journal of Heat and Fluid Flow*, vol. 78, 2019. [Online]. Available: https://doi.org/10.1016/j.ijheatfluidflow.2019.108426

[31] L. Jégo and S. Guillou, "Study of a Bi-Vertical Axis Turbines Farm Using the Actuator Cylinder Method," *Energies*, vol. 14, no. 16, p. 5199, aug 2021. [Online]. Available: https://doi.org/10.3390/en14165199

[32] G. Deskos, G. S. Payne, B. Gaurier, and M. Graham, "On the spectral behaviour of the turbulence-driven power fluctuations of horizontal-axis turbines," *Journal of Fluid Mechanics*, vol. 904, p. A13, dec 2020. [Online]. Available: https://doi.org/10.1017/jfm.2020.681